Comparison of Reference Sensor Types and Position for Motion Artifact Removal in ECG

Jannis Lilienthal and Waltenegus Dargie
Technische Universität Dresden
01062 Dresden, Germany
{jannis.lilienthal, waltenegus.dargie}@tu-dresden.de

***Abstract*—Wireless electrocardiograms (WECGs) allow long-term monitoring of patients in their residential and work environments. However, the measurements are easily affected by motion artifacts. To reason about and remove the artifacts, reference models (signals) are needed. One way to construct these models is by employing motion sensors that pick up the motion affecting the electrodes of a WECG. In this paper, we experimentally examine the existence of correlations between the measurements of inertial sensors and motion artifacts. We employed three reference sensor types (3D accelerometer, 3D gyroscope, and skin impedance sensor). Our analysis includes actual measurements taken from eleven healthy subjects carrying out six different movements: Stand up, bend forward, walking, running, jumping and climbing stairs. We found that the best place to attach inertial sensors is the sternum of the torso. Although all three sensor types exhibit comparable levels of correlation to isolated motion artifacts, the gyroscope performs best in removing motion artifacts with an adaptive filter.**

***Index Terms*—Accelerometer, adaptive filter, electrocardiogram, gyroscope, impedance, inertial sensor, motion artifact**

I. Introduction

Detecting and treating diseases belonging to the group of Cardiovascular diseases (CVDs) is one of the most important challenges facing the healthcare system in the 21st century. These diseases are characterized by high mortality and morbidity, thereby accounting for 17.9 million deaths every year [1]. Their detection and monitoring are therefore vital in order to initiate the correct treatment.

Recent advances in telemedicine have provided mobile devices that offer continuous monitoring of cardiac activity. Wireless electrocardiograms (WECGs) can be employed outside of clinical settings to monitor cardiovascular health for subjects in risk groups to detect anomalies that occur suddenly or episodically (e.g., occult arrhythmia, which are paroxysmal, transient, and appearing in particular situations [2]). Furthermore, remote monitoring can help patients in risk groups maintain an independent lifestyle while ensuring that their health is closely monitored.

The WECG is obtained by attaching electrodes on the skin surface and measuring the potential difference in between. Rhythmic contractions of the heart muscle generate action potentials, which are then picked up by these electrodes. Unfortunately, these measurements are regularly affected by different noise types: muscle noise, baseline wander, powerline interference, and motion artifacts. One of the most challenging distortions are motion artifacts because their spectrum and magnitude overlap the cardiac information delivered [3]. Their appearance can cause significant diagnostic errors ranging from falsely diagnosed arrhythmia to resembling pathological conditions such as atrial flutter/fibrillation [4].

Many methods have been proposed to remove motion artifacts from WECG: wavelet denoising [5]–[7], blind source separation [8], [9], and neural networks [10]. The adaptive filter remains the most commonly used method for artifact removal, despite the recent advances in signal processing. It estimates the motion artifacts in the electrocardiogram (ECG) by employing a reference signal correlated to the noise. The low energy consumption and simplicity make its application expedient for mobile monitoring [11], [12]. These monitoring devices usually consist of sensors to measure the ECG but also integrate an inertial measurement unit (IMU) to characterize the movements performed. The IMU contains an accelerometer and a gyroscope to record three-dimensional acceleration and rotational velocity, respectively. Complementary to the inertial sensors, the skin-electrode impedance can be recorded by inducing a low alternating current and measuring its motion-induced variation.

The skin-electrode impedance [13], [14] and the accelerometer [14], [15] represent two well-established reference sensors investigated. Although IMUs typically incorporate a gyroscope, this type of sensor has not been examined in the literature for its ability to remove motion artifacts.

In the following, we examine the relationship between the three sensor types available and isolated motion artifacts to identify the sensor that correlates best with the artifacts and removes them from the signal in the best possible way. Furthermore, a motion affects different parts of the body differently, thereby making the deployment of motion sensors to model and reason about motion artifacts challenging. In this paper, we investigate:

- the extent to which the measurements of motion sensors correlate with motion artifacts, and;
- how the placement of sensors influences the analysis of motion artifacts.

This work has been funded by the German Research Foundation (DFG) under the project agreements DA 1211/7-1 (RoReyBaN).

II. Material and Methods

The following section provides a detailed description of the experimental setup and processing step employed and the methodology to compare the reference sensors.

To reason about motion artifacts removal in ECG, many approaches employ the MIT-BIH database that contains, among others, noise-free ECG and recordings of isolated motion artifacts [16]. Artificially corrupted ECGs can subsequently be generated by combining the artifacts and the noise-free ECG segments. Unfortunately, this database does not contain any information on the movement types executed, nor does it include the data from reference sensors to characterize the movements. Therefore, we designed our own experimental setup to (1) record ECG corrupted by motion and (2) characterize the relationship between reference sensors and the motion artifacts. We employed the Shimmer3 platform [17] which provides the synchronous measurement of the ECG, a 3D accelerometer, and a 3D gyroscope. Furthermore, the skin-electrode impedance can be measured between a pair of electrodes by injecting an alternating current ($f_{mod} = 32\,\mathrm{kHz}$ and $I_{Imp} = 30\,\mu\mathrm{A}$).

For each experiment, we employed five Shimmer3 nodes per person. We deployed them in different locations in the torso region and at the back: One of the nodes was placed at the chest, at the height of the sternum. Three nodes were placed as close as possible to the wet ECG electrodes (Kenndal, H135SG): left arm (LA), right arm (RA), and left leg (LL). The skin was prepared using alcohol wipes to clean the contact area. All leads were fixed to the torso with surgical tapes to minimize localized motion. Figure 1 illustrates the sensor arrangement.

The ECG can be recorded either in motion or at rest. When the subject is in motion, the information retrieved on the skin surface contains the cardiac information mixed with the motion artifacts according to an unknown function $f(v)$. Without the exact knowledge of the mixing process, they cannot be separated with 100% accuracy, and analyzing their characteristics is not straightforward. To record isolated motion artifacts with minimal cardiac influence, we attached an additional sensor node at the back of each subject. Figure 1 illustrates the arrangement of the bias (B), reference (R), and positive (P) electrodes at the back. By suppressing cardiac action potentials this way, it is possible to investigate the relationship between (a) the motion artifacts generated by motion alone and (b) the output of the motion sensors.

Attaching inertial sensors to capture motion artifacts inadvertently interferes with the body's function and external structure. Sensors attached near the electrodes push and pull them during movement because of the extra weight they introduce to the skin's surface. This effect generates its own motion artifacts. In order to minimize this effect, we introduced a minimum distance between the electrodes and the sensor platforms, but in doing so, we also limited the sensors' ability to measure the motion directly affecting the electrodes accurately.

We recorded data from eleven healthy subjects undertaking a selection of everyday activities. We deliberately included high-intensity (running, jumping, climbing stairs) and light-intensity movements (standing up, bending forward, and walking). Thereby, we wish to address the different characteristics of movements and how these translate to the correlation to reference sensors. We tried to make the execution of the motions as natural as possible. Only bending forward, standing up from a chair, and jumping were performed on the spot. For the remaining movements, no restrictions were made on the pace or magnitude of the execution, and the subjects were able to move freely while performing the respective movement type. We recorded 120 s for each movements at a sampling rate of $f_s = 512\,\mathrm{Hz}$. The raw data was subsequently bandpass filtered in the range of 0.05–150 Hz following the American Heart Association (AHA) recommendations for the standardization in ECG analysis.

III. Results and Discussion

We divide this section into three subsections. First, we investigate the influence of sensor placement on the correlation between inertial sensors and noisy ECG. We then compare the extent to which the different motion sensors' outputs are correlated with the isolated motion artifacts (measured at the back of a subject) and determine their ability to remove these artifacts from noisy ECG.

Figure 2 displays sample inertial measurements and the associated ECG/motion artifacts recorded at the back while bending forward. A cursory look suggests that the measurements are correlated. We wish to quantify the prevalence of this feature in different subjects and movement types. Therefore, we employed

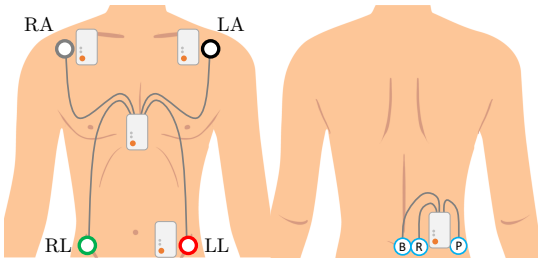

Figure 1. Electrode and sensor location at the front and the back of the subjects.

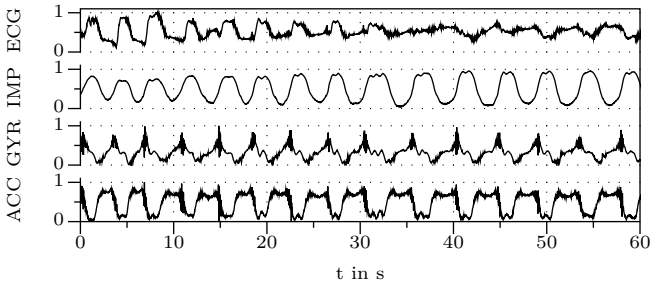

Figure 2. An example of the electrocardiogram at the back and the reference sensors for one subject performing the movement bending.

a moving window cross-correlation – the correlation between two zero-mean time-shifted signals – defined as:

$$R_{xy}(m) = \mathrm{E}[x_{n+m} y_n^*] \tag{1}$$

where E is the expected value and x and y are two time-series. We subsequently normalized the cross-correlation so that the autocorrelations of x and y at zero lag are equal to one, and the cross-correlation can attain values in $R_{xy} \in [-1; 1]$. Because we are interested in the relation between the motion artifacts and the reference sensors under the best possible conditions, we employ the maximum absolute cross-correlation – $R_{max} = \max |R_{xy}|$ in the following. Moreover, for the comparisons we make, we shall consider the median of R_{max} along with the median absolute deviation (MAD) to reduce the influence of outliers in the dataset.

A. Impact of Sensor Placement

In this section, we investigate the impact of sensor placement on the strength of the correlation. Our focus will be on the correlation between the motion sensors and the noisy ECG (lead I). We thereby wish to investigate whether placing the inertial sensors next to the ECG electrodes can enhance the correlation to the noisy ECG or whether it is sufficient to use a single sensor.

The gyroscope and the accelerometer record three-dimensional angular velocity (rotational motion) and linear acceleration, respectively. In general, these sensor axes score different correlation-coefficients since they are affected differently by one and the same movement. For our comparison, for each sensor, we select only one of the axes for which the absolute cross-correlation is the best:

$$|R|_{max,xcorr} = \max_{axis \in \{x,y,z\}} \{|R|_{max,xcorr,axis}\} \tag{2}$$

The time lag of the cross-correlation was limited to one second. Subsequently, the cross-correlation is calculated between the noisy ECG and each axis of the accelerometer or gyroscope, respectively. Thus, $R_{max,xcorr}$ denotes the highest cross-correlation observed over the three orthogonal axes of one sensor type.

Figure 3 displays the values of $|R|_{max,xcorr}$ for the different types of movements and different sensor placements. The sensor in question is the accelerometer. Overall, the motion sensors' outputs are well correlated with the noisy ECG for bending, jumping, and running (the first two exhibiting median correlation coefficients greater than 0.4). Walking and running are also the types of movements for which sensor placement matters. In all of them, the sensors placed at the back and the hip result in weaker correlations, while the sensors placed in the upper part of the body score comparatively high but similar correlations. Standing up and climbing the staircase resulted in relatively weak overall correlation coefficients, but sensor placement does not seem to affect the former significantly.

Figure 4 displays the cross-correlation coefficients for the gyroscope experiments. Like the experiments with accelerometers, overall, bending, running, and jumping exhibit high correlations, and standing up and climbing structures small correlations. Sensor placement appears to matter for walking, running, jumping, and climbing stairs, all of which require translational motions.

Discussion: Three conclusions can be made from the above results:

1) While placing motion sensors in the upper body is advantageous (compared to placing them at the hip or the back), there is no apparent advantage in placing them near the electrodes of the WECG.
2) Because of the comparable results we observe between the three sensor placements (LA, RA, center), it can be construed that the motion artifacts we can measure using inertial sensors are more likely the results of macro body movements as opposed to localized electrode movements.
3) Gyroscopes are more sensitive to sensor placement compared to accelerometers.

B. Correlation to Isolated Artifacts

Figure 5 expresses the correlation between the three sensors and the artifacts recorded at the back. Climbing stairs exhibits the weakest correlation for all sensor types. By comparison, bending forward scores the strongest correlation with $R_{max} > 0.5$ and little deviation across sensor types. The remaining movements (standing up, walking, running, and jumping) score similar correlation coefficients. Notable differences among the sensors are present for walking, running,

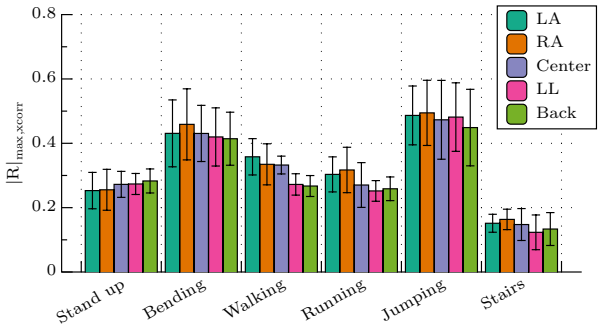

Figure 3. Median of the maximum cross-correlation coefficient between different accelerometer positions and the ECG-lead I.

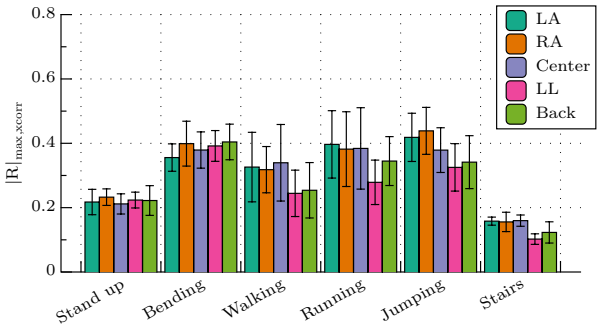

Figure 4. Median of the maximum cross-correlation coefficient between different gyroscope positions and the ECG-lead I.

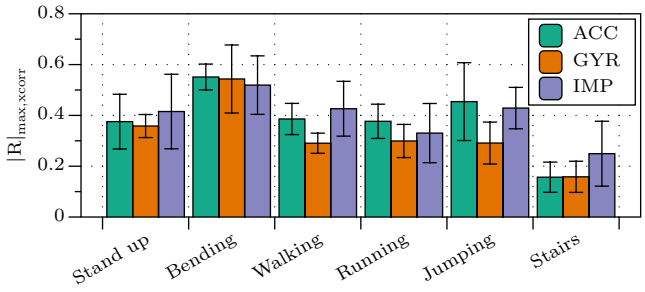

Figure 5. Median of the maximum cross-correlation coefficient between the reference and the artifact at the back.

and jumping, for which the gyroscope scores the weakest correlation coefficient. Overall, the accelerometer and the impedance sensor correlate better with the artifacts for most of the movements.

From our analysis, it can be construed that no single sensor stands out in picking up motion artifacts in all the cases we considered, but the impedance sensor and the accelerometer performed comparatively well. The correlation coefficients we present for the impedance sensor are partially consistent with the results of Buxi et al. [18]. However, in their study they present a maximum correlation for running of $R_{max} = 0.6$ which significantly differs from our results ($R_{max} = 0.3$). The origin of this deviation is likely manifold: measurement duration ($t_{m,Buxi} = 60\,\text{sec}$ vs. $t_m = 120\,\text{sec}$), execution (on the spot vs. translational) or impedance frequency ($f_{imp} = 2.2\,\text{kHz}$ vs. $f_{imp} = 32\,\text{kHz}$).

C. Application to Motion Artifact Removal

In the following, we investigate how the differences in correlation are reflected in the removal of motion artifacts. We thereby wish to determine if one sensor type performs significantly better than the others. Therefore, we employed an least mean square adaptive filter (LMS-AF), commonly used to remove motion artifacts from ECG measurements.

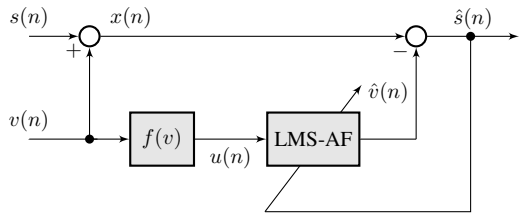

Figure 6. Block diagram of an adaptive filter for motion artifact removal.

The LMS-AF automatically adapts its filter coefficients to minimize an error function, in this case, provided by the least mean square (LMS) error. Therefore, a reference input $u(n)$ is required, which is ideally well correlated to the motion artifacts $v(n)$. Subsequently the filter coefficients are optimized with regard to the LMS error between the noisy ECG $x(n)$ and the output of the LMS-AF $\hat{v}(n)$ to generate an estimation of the artifact-free ECG $\hat{s}(n)$. The underlying assumption is that the reference sensor and the motion artifacts in the ECG are correlated, and the cardiac information and the motion artifacts are uncorrelated. Figure 6 illustrates the framework of an adaptive filter to remove motion artifacts from the ECG.

We generated artificially corrupted ECG with a known signal-to-noise ratio (SNR) between −10 to 5 dB by combining the isolated artifacts recorded at the back and clean ECG segments recorded in rest. This way, it is possible to compare the results for the particular reference sensors objectively. To evaluate the performance, we considered the SNR and the root mean squared error (RMSE):

$$\text{SNR}_{dB} = 10 \cdot \log_{10}\left(\frac{P_{\text{signal}}}{P_{\text{noise}}}\right) \tag{3}$$

$$\text{RMSE} = \sqrt{\frac{1}{n}\sum_{i=1}^{n}(s_i - \hat{s}_i)^2} \tag{4}$$

where P_{signal} is the power of the cardiac information in the ECG and P_{noise} is the power of the noise, i.e., the motion artifacts. The RMSE is subsequently calculated between the noise free ECG s and the estimated noise-free ECG $\hat{s}$ generated by the filter. The step-size μ influences performance of the LMS-AF significantly. A large step-size ($\mu = 0.1$) increases the convergence speed but can introduce distortions into the signal, even though the motion artifacts are marginal. On the other hand, a small step-size ($\mu = 0.01$) introduces negligible distortion but converges slowly and therefore fails to track fastly changing motion artifacts. Unfortunately, the step-size applied in the literature is not consistent ($\mu = 0.01$ [19], $\mu = 0.08$ [20]). Therefore, we reviewed the performance for different step sizes by considering $\mu \in [0.01; 0.1]$. We subsequently analyzed the results with regard to the SNR and RMSE to select an appropriate step-size for each sensor type. We found that the following step-sizes performed best: $\mu_{acc} = 0.07$, $\mu_{gyr} = 0.07$ and $\mu_{imp} = 0.06$.

Table I
COMPARISON OF THE PERFORMANCE FOR DIFFERENT REFERENCE SENSORS.

Sensor	**SNR** in dB		**RMSE**	
	before	after	before	after
Impedance	-10	-5.2	0.159	0.216
	-5	-2.6	0.131	0.163
	0	-1.3	0.095	0.141
	5	-0.7	0.062	0.133
Accelerometer	-10	-2.4	0.159	0.167
	-5	-1.2	0.131	0.144
	0	-0.4	0.095	0.133
	5	-0.1	0.062	0.127
Gyroscope	-10	-1.4	0.159	0.146
	-5	-0.5	0.131	0.131
	0	-0.1	0.095	0.126
	5	0.0	0.062	0.124

Table I displays the results for the LMS-AF as mean values over the six movement types and eleven subjects considered. Although the previous results suggested that all sensors perform on a comparable level, the SNR and the RMSE after applying

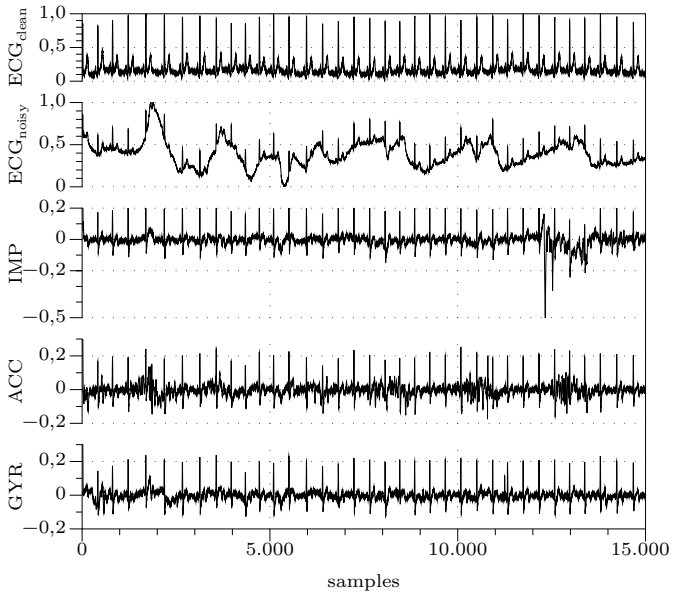

Figure 7. Comparison of motion artifact removal in ECG for three different reference sensors.

the algorithms indicate that the gyroscope outperforms the other sensor for all noise levels regarded.

Figure 7 depicts the results of motion artifact removal for a generically chosen subject. The results are consistent with our numeric evaluation – all available reference sensors remove the artifacts to a certain extent. However, there are fine-grained differences in the performance and characteristics of the particular sensors. The gyroscope removes most of the artifacts and produces a clean signal without protruding points. On the other side, both the skin-electrode impedance and the accelerometer remove motion artifacts but also introduce significant signal distortion into the measurements. The disturbances caused by the accelerometer appear predominantly in high frequency but low amplitude components. The distortion introduced by the skin-electrode impedance is around 200% of the R peak amplitude and is likely located in the same spectral range.

IV. Conclusion

In this paper, we examined the correlations between motion artifacts superimposed on the measurements of a WECG and different types of motion sensors (3D accelerometer, 3D gyroscope, and skin-impedance sensor). We employed Shimmer3 sensor platforms and experimented with six different types of stationary and translational movements. Our analysis focused on the sensors' capacity and the placement of the sensors to capture motion artifacts. Our observation indicates that all the sensors we considered captured artifacts to certain extents, depending on the movement types. The position that registered the best correlation coefficients for most movements was the center of the torso (sternum). There is no apparent advantage in placing the sensors next to the electrodes. The gyroscope outperforms the other reference sensors in removing motion artifacts from the ECG. It results in a higher SNR and a lower RMSE for all noise levels considered.

References

[1] World Health Organization, "Global Health Estimates 2016: Deaths by Cause, Age, Sex, by Country and by Region, 2000-2016. Geneva: WHO, 2018," World Health Organization, Geneva, Tech. Rep., 2019.

[2] P. Xiong, H. Wang, M. Liu, *et al.*, "A stacked contractive denoising auto-encoder for ECG signal denoising," *Physiological Measurement*, vol. 37, no. 12, pp. 2214–2230, Dec. 2016.

[3] N. V. Thakor, J. G. Webster, and W. J. Tompkins, "Estimation of QRS Complex Power Spectra for Design of a QRS Filter," *IEEE Transactions on Biomedical Engineering*, vol. BME-31, no. 11, pp. 702–706, Nov. 1984.

[4] S. I. Patel, M. J. Souter, D. S. Warner, *et al.*, "Equipment-related Electrocardiographic Artifacts," *Anesthesiology*, vol. 108, no. 1, pp. 138–148, 2008.

[5] S. Nagai, D. Anzai, and J. Wang, "Motion artifact removal for wearable ECG using stationary wavelet multi-resolution analysis," in *2017 IEEE 5th International Symposium on Electromagnetic Compatibility (EMC-Beijing)*, vol. 2017-Octob, IEEE, Oct. 2017, pp. 1–5.

[6] ——, "Motion artefact removals for wearable ECG using stationary wavelet transform," *Healthcare Technology Letters*, vol. 4, no. 4, pp. 138–141, Aug. 2017.

[7] F. Strasser, M. Muma, and A. M. Zoubir, "Motion artifact removal in ECG signals using multi-resolution thresholding," *European Signal Processing Conference*, no. Eusipco, pp. 899–903, 2012.

[8] J. Lilienthal and W. Dargie, "Application of Tensor Decomposition in Removing Motion Artifacts from the Measurements of a Wireless Electrocardiogram," in *2020 IEEE 23rd International Conference on Information Fusion (FUSION)*, IEEE, Jul. 2020, pp. 1–8.

[9] M. Milanesi, N. Martini, N. Vanello, *et al.*, "Independent component analysis applied to the removal of motion artifacts from electrocardiographic signals," *Medical & Biological Engineering & Computing*, vol. 46, no. 3, pp. 251–261, Mar. 2008.

[10] S. Poungponsri and X.-H. Yu, "An adaptive filtering approach for electrocardiogram (ECG) signal noise reduction using neural networks," *Neurocomputing*, vol. 117, pp. 206–213, Oct. 2013.

[11] N. Van Helleputte, S. Kim, H. Kim, *et al.*, "A 160 μ a biopotential acquisition IC with fully integrated IA and motion artifact suppression," *IEEE Transactions on Biomedical Circuits and Systems*, vol. 6, no. 6, pp. 552–561, 2012.

[12] N. Van Helleputte, M. Konijnenburg, J. Pettine, *et al.*, "A 345 μw multi-sensor biomedical SoC with Bio-impedance, 3-Channel ECG, motion artifact reduction, and integrated DSP," *IEEE Journal of Solid-State Circuits*, vol. 50, no. 1, pp. 230–244, 2015.

[13] H. Zhang, S. Zhang, X. Du, *et al.*, "A multi-channel electrode tissue impedance detection approach for motion artifact suppression in ambulatory electrocardiography," *Computing in Cardiology*, vol. 42, no. February 2016, pp. 117–120, 2015.

[14] I. Romero, D. Geng, and T. Berset, "Adaptive filtering in ECG denoising: A comparative study," *Computing in Cardiology*, vol. 39, pp. 45–48, 2012.

[15] S. W. Yoon, S. D. Min, Y. H. Yun, *et al.*, "Adaptive motion artifacts reduction using 3-axis accelerometer in E-textile ECG measurement system," *Journal of Medical Systems*, vol. 32, no. 2, pp. 101–106, Apr. 2008.

[16] G. B. Moody, W. K. Muldrow, and R. G. Mark, *Noise Stress Test for Arrhythmia Detectors.* 1984.

[17] A. Burns, B. R. Greene, M. J. McGrath, *et al.*, "SHIMMER - A wireless sensor platform for noninvasive biomedical research," *IEEE Sensors Journal*, vol. 10, no. 9, pp. 1527–1534, Sep. 2010.

[18] D. Buxi, S. Kim, N. Van Helleputte, *et al.*, "Correlation between electrode-tissue impedance and motion artifact in biopotential recordings," *IEEE Sensors Journal*, vol. 12, no. 12, pp. 3373–3383, 2012.

[19] L. M. Bai, M. H. Fan, C. H. Feng, *et al.*, "Using an Adaptive Filter to Remove ECG Motion Artifact Interference," *2018 IEEE International Conference on Consumer Electronics-Taiwan, ICCE-TW 2018*, pp. 1–2, 2018.

[20] H. Kim, S. Kim, N. Van Helleputte, *et al.*, "Motion artifact removal using cascade adaptive filtering for ambulatory ECG monitoring system," in *2012 IEEE Biomedical Circuits and Systems Conference (BioCAS)*, IEEE, Nov. 2012, pp. 160–163.